

## **FAST CALCULATION OF WIDE-BAND RESPONSES OF COMPLEX RADAR TARGETS**

**S. G. Wang, X. P. Guan, D. W. Wang, X. Y. Ma, and Y. Su**

School of Electronic Science and Technology  
National University of Defense Technology  
Changsha 410073, China

**Abstract**—In this paper, a fast method is proposed to calculate wide-band frequency responses of complex radar targets on a personal computer. When frequencies are low, the frequency factor can be separated from space parameters by Chebyshev polynomial approximations of Green's function. Then, matrices from MoM at different frequencies can be rapidly filled, and monostatic RCS can be soon calculated. If frequencies are relatively high, a fast high-order MoM (HO-MoM), in which matrices products are in place of multi-dimension numerical integrations, is presented. That will reduce the CPU time requirement. Lastly, Numerical results are given for various structures and compared with other available data.

### **1. INTRODUCTION**

Scattering by arbitrarily shaped conducting objects can be converted to finding the solution of an integral equation where the unknown is the induced current distribution. The integral equation can be solved by the method of moments (MoM). The resultant matrix equation requires  $O(N^3)$  floating-point operations, and is memory consuming. The fast multipole method (FMM) and multilevel fast multipole algorithm (MLFMA) [1–3] are broadly used to solve the matrix equation for reducing the calculating complexity. Recently, the high-order MoM (HO-MoM) [4, 5] is proposed in electromagnetic scattering.

For calculating wide-band frequency responses of complex radar targets, the matrix will be repeatedly filled at each frequency point. That is very time-consuming even using FMM and MLFMM. The technology of asymptotic waveform evaluation (AWE) [6] and model-based parameter estimation (MBPE) [7] combined with MoM are usually used to calculate monostatic RCS over a wide frequency band.

That is much more efficient than the conventional point-by-point approach. But, when the frequency band and the order of current in AWE or MBPE are not appropriately chosen, the precision of results will be low.

In this paper, a fast method is proposed to calculate wide-band frequency responses of complex radar targets on a personal computer. In the low frequency band, the frequency factor can be separated from space parameters by Chebyshev polynomial approximation of Green's function. Those, which have something to do with the geometrical parameters of scatters, are calculated and stored first. Then, matrices from MoM at different frequencies can be rapidly filled, and monostatic RCS versus frequencies can be soon calculated. In the relative high frequency band, a fast high-order MoM (HO-MoM), in which matrices products are in place of multi-dimension numerical integrations, is presented. That will reduce the CPU time requirement.

## 2. BASIC THEORY OF MOM

For RCS calculation of an arbitrarily shaped PEC body, a plane wave is assumed to be incident at an angle  $(\theta_i, \varphi_i)$ . The incident field is  $\mathbf{E}_{inc}$ , and the scattering field is  $\mathbf{E}_{scat}$ . On the surface of the PEC body the total tangential electric field is zero. The total tangential field in terms of the scattered and incident fields on the PEC body is therefore written as

$$[\mathbf{E}_{scat} + \mathbf{E}_{inc}]_{\tan} = 0 \quad (1)$$

The scattering field is

$$\mathbf{E}_{scat} = -j\omega\mathbf{A}(\mathbf{r}) - \nabla\Phi(\mathbf{r}) \quad (2)$$

$\mathbf{A}(\mathbf{r})$  and  $\Phi(\mathbf{r})$  are respectively the magnetic vector potential and electric scalar potential, given by

$$\mathbf{A}(\mathbf{r}) = \frac{\mu}{4\pi} \int_s \mathbf{J}(\mathbf{r}') \frac{\exp(-jkR)}{R} ds' \quad (3)$$

$$\Phi(\mathbf{r}) = -\frac{1}{4\pi j\omega\epsilon} \int_s \nabla'_s \cdot \mathbf{J}(\mathbf{r}') \frac{\exp(-jkR)}{R} ds' \quad (4)$$

where  $\mathbf{J}$  is the equivalent electric current.  $\nabla'$  indicates the del operation over the source coordinates and similarly  $ds'$  indicates the surface integration over the source coordinates.  $\omega$  is the frequency in radians per second.  $R$  is the distance between the source point and the observation point.  $\epsilon$  and  $\mu$  are the permittivity and permeability in free space. The propagation constant is

$$k = [\omega^2 \mu \epsilon]^{1/2} \quad (5)$$

In a subdomains MoM approach, the surface of an object is divided into triangles, rectangles, or quadrilaterals. Galerkin's MoM method applied, a set of simultaneous equations is generated and written in a matrix equation form as

$$\mathbf{Z}\mathbf{I} = \mathbf{V} \quad (6)$$

where  $\mathbf{Z} = [Z_{mn}]$  is an  $N \times N$  matrix and  $\mathbf{I} = [I_n]$  and  $\mathbf{V} = [V_m]$  are column vectors of length  $N$ .

If the RWG basis functions  $\{\mathbf{f}_n(\mathbf{r}')\}$  are used in MoM, elements of  $\mathbf{Z}$  are given by

$$Z_{mn} = l_m \left[ j\omega \left( \mathbf{A}_{mn}^+ \cdot \frac{\boldsymbol{\rho}_m^{c+}}{2} + \mathbf{A}_{mn}^- \cdot \frac{\boldsymbol{\rho}_m^{c-}}{2} \right) + \Phi_{mn}^- - \Phi_{mn}^+ \right] \quad (7)$$

where

$$\mathbf{A}_{mn}^\pm = \frac{\mu}{4\pi} \int_s \mathbf{f}_n(\mathbf{r}') \frac{e^{-jkR_m^\pm}}{R_m^\pm} ds' \quad (8)$$

$$\Phi_{mn}^\pm = \frac{-1}{4\pi j\omega\epsilon} \int_s \nabla'_s \cdot \mathbf{f}_n(\mathbf{r}') \frac{e^{-jkR_m^\pm}}{R_m^\pm} ds' \quad (9)$$

The symbols in (7), (8) and (9) are the same as those in [8].

In high-order MoM (HO-MoM), the surface are usually divided into quadrilaterals, over which electric current density vectors are represented as

$$\mathbf{J}_s(u, v) = \sum_{i=0}^{N_u} \sum_{j=0}^{N_v-1} \beta_{uij} \mathbf{f}_{uij}(u, v) + \sum_{i=0}^{N_u-1} \sum_{j=0}^{N_v} \beta_{vij} \mathbf{f}_{vij}(u, v) \quad (10)$$

where

$$\mathbf{f}_{uij}(u, v) = \frac{P_i(u)v^j}{J(u, v)} \mathbf{a}_u(u, v) \quad (11)$$

$$\mathbf{f}_{vij}(u, v) = \frac{u^i P_j(v)}{J(u, v)} \mathbf{a}_v(u, v) \quad (12)$$

$$P_i(u) = \begin{cases} 1 - u, & i = 0 \\ 1 + u, & i = 1 \\ u^i - 1, & i \geq 2, \text{ even} \\ u^i - u, & i \geq 3, \text{ odd} \end{cases}$$

$$\mathbf{a}_u(u, v) = \frac{\partial \mathbf{r}(u, v)}{\partial u}, \quad \mathbf{a}_v(u, v) = \frac{\partial \mathbf{r}(u, v)}{\partial v} \quad (13)$$

Parameters  $N_u$  and  $N_v$  are the adopted degrees of the polynomial current approximation,  $\beta_{uij}$  and  $\beta_{vij}$  are unknown coefficients.  $\mathbf{a}_u$

and  $\mathbf{a}_v$  are unitary vectors.  $\mathbf{r}(u, v)$  describes the quadrilateral by parametric coordinates.

In HO-MoM, elements of  $\mathbf{Z}$  are given by [5]

$$\begin{aligned} \mathbf{Z}(i_m, j_m, i_n, j_n) = & -j\omega\mu \sum_{k_m=1}^{p^{(m)}} \sum_{l_m=0}^{p^{(m)}} \sum_{k_n=1}^{p^{(n)}} \sum_{l_n=0}^{p^{(n)}} k_m k_n \mathbf{r}_{k_m l_m}^{(m)} \\ & \cdot \mathbf{r}_{k_n l_n}^{(n)} \xi(i_m + k_m - 1, j_m + l_m, i_n + k_n - 1, j_n + l_n) \\ & - \frac{1}{j\omega\varepsilon} \zeta(i_m - 1, j_m, i_n - 1, j_n) \end{aligned} \quad (14)$$

where, superscript  $m$  and  $n$  respectively indicate the  $m$ th patch and the  $n$ th patch, on which  $p^{(m)}$  and  $p^{(n)}$  are geometrical orders along parametric coordinate, and

$$\xi(i_m, j_m, i_n, j_n) = \int_{-1}^1 \int_{-1}^1 \int_{-1}^1 \int_{-1}^1 u_m^{i_m} v_m^{j_m} u_n^{i_n} v_n^{j_n} g(R) du_n dv_n du_m dv_m. \quad (15)$$

Usually,  $N_u = N_v = M$ ,  $0 \leq i_m, j_m, i_n, j_n \leq M$  and  $g(R) = \frac{e^{-jkR}}{R}$ .

After (6) is solved, responses can be easily calculated through (2).

### 3. POLYNOMIAL APPROXIMATION IN MOM

In (8) and (9), the factor of frequency only exists in the form as  $e^{-jkR}$ , which can be approximated by polynomial series. Chebyshev polynomial approximation is a better one, the error of which is equally distributing. The approximation follows as

$$e^{-jkR} = \sum_{p=0}^P a_p R^p + TR_P \quad (16)$$

where  $P$  is the maximal number of polynomials.  $a_p$  ( $p = 0, 1, \dots, P$ ) are coefficients of polynomials, and  $TR_P$  is the truncation error.

On substituting the relationships (16) into (8) and (9). The potential functions are obtained as

$$\mathbf{A}_{mn}^{\pm} = \frac{\mu}{4\pi} \sum_{p=0}^P a_p \int_s \mathbf{f}_n(\mathbf{r}') (R_m^{\pm})^p ds' \quad (17)$$

$$\Phi_{mn}^{\pm} = \frac{-1}{4\pi j\omega\varepsilon} \sum_{p=0}^P a_p \int_s \nabla'_s \cdot \mathbf{f}_n(\mathbf{r}') (R_m^{\pm})^p ds' \quad (18)$$

Let

$$\mathbf{A}_{mn,p}^{\pm} = \frac{\mu}{4\pi} \int_s \mathbf{f}_n(\mathbf{r}') (R_m^{\pm})^p ds' \quad (19)$$

$$\Phi_{mn,p}^{\pm} = \frac{-1}{4\pi\epsilon} \int_s \nabla'_s \cdot \mathbf{f}_n(\mathbf{r}') (R_m^{\pm})^p ds' \quad (20)$$

So the impedance matrix will be in the form as

$$\begin{aligned} Z_{mn} = l_m & \left[ j\omega \left( \sum_{p=0}^P a_p \left( \mathbf{A}_{mn,p}^+ \cdot \frac{\boldsymbol{\rho}_m^{c+}}{2} + \mathbf{A}_{mn,p}^- \cdot \frac{\boldsymbol{\rho}_m^{c-}}{2} \right) \right) \right] \\ & + \frac{l_m}{j\omega} \sum_{p=0}^P a_p (\Phi_{mn,p}^- - \Phi_{mn,p}^+) \end{aligned} \quad (21)$$

where  $\mathbf{A}_{mn,p}^{\pm}$  and  $\Phi_{mn,p}^{\pm}$  have nothing to do with frequencies. When  $p = 0$ , (19) and (20) are evaluated by accurate analytical method over the triangular surface. When  $p > 0$ , the Gauss-Legendre integration formulas is employed in (19) and (20). At different frequencies, the coefficients of polynomials in (16) are only repeatedly evaluated, and the matrix will be filled rapidly by (21).

#### 4. FAST ALGORITHM IN HO-MOM

If the source patch (the  $m$ th patch) is not the same as the field patch (the  $n$ th patch), the numerical integration of (15) will be repeatedly calculated. In HO-MoM, the direct calculation of the four-dimensional integration is time-consuming. When the number of patches and the current expanding order are large, the matrix-filled time is unendurable. In this part, the multi-dimensional integrations are computed by matrices products.

Because the independent variables in each dimension of (15) are mutually irrelative, the numbers of each dimensional integral nodes can be chosen respectively as  $N_{Gum}$ ,  $N_{Gvm}$ ,  $N_{Gun}$  and  $N_{Gvn}$ , which yield [9]

$$N_{Gum} \geq M + 1, N_{Gvm} \geq M + 1, N_{Gun} \geq M + 1, N_{Gvn} \geq M + 1.$$

In this paper, the numbers of nodes are selected as that

$$N_{Gum} = N_{Gvm} = N_{Gun} = N_{Gvn} = M + 1.$$

The nodes of one dimension Gauss-Legendre integration are written in vector form,  $[x_k]_{(M+1) \times 1}$ . The corresponding coefficient vector is

$[A_k]_{(M+1) \times 1}$ . (15) is numerically computed,

$$\xi(i_m, j_m, i_n, j_n) = \sum_{c=0}^M \sum_{d=0}^M \sum_{e=0}^M \sum_{f=0}^M A_c A_d A_e A_f u_{mc}^{i_m} v_{md}^{j_m} u_{ne}^{i_n} v_{nf}^{j_n} g(R(u_{mc}, v_{md}, u_{ne}, v_{nf})) \quad (22)$$

where  $u_{mc}, v_{md}, u_{ne}, v_{nf} \in [x_k]_{(M+1) \times 1}$ , and  $A_c A_d A_e A_f \in [A_k]_{(M+1) \times 1}$ .

In (22), the nodes and coefficients in Gauss-Legendre integration are invariant. Green's function,  $g(R)$ , is only calculated. So, the matrix  $\mathbf{Z}_{uv}$  is defined to store the coefficients. The elements of  $\mathbf{Z}_{uv}$  yield

$$Z_{uv}(p, q) = A_c A_d A_e A_f u_{mc}^{i_m} v_{md}^{j_m} u_{ne}^{i_n} v_{nf}^{j_n} \quad (23)$$

where,

$$p = i_m(M+1)(M+1)(M+1) + j_m(M+1)(M+1) + i_n(M+1) + j_n \quad (24)$$

$$q = c(M+1)(M+1)(M+1) + d(M+1)(M+1) + e(M+1) + f \quad (25)$$

What's more, a vector  $\mathbf{GR}$  is defined to store the values of Green's function at integral nodes. The length is  $(M+1)(M+1)(M+1)(M+1)$ , and the elements are that

$$\mathbf{GR}(q) = \frac{e^{-jkR_q}}{R_q} \quad (26)$$

where,  $q$  yields (25), and  $R_q(u_{mc}, v_{md}, u_{ne}, v_{nf}) = |\mathbf{r}_{mq} - \mathbf{r}_{nq}|$ . On bilinear quadrilateral patches, the source point and observation point are respectively [10]

$$\mathbf{r}_{mq} = \mathbf{r}_{cm} + u_{mc}\mathbf{r}_{um} + v_{md}\mathbf{r}_{vm} + u_{mc}v_{md}\mathbf{r}_{uvm} \quad (27)$$

$$\mathbf{r}_{nq} = \mathbf{r}_{cn} + u_{ne}\mathbf{r}_{un} + v_{nf}\mathbf{r}_{vn} + u_{ne}v_{nf}\mathbf{r}_{uvn} \quad (28)$$

Let

$$\mathbf{T} = \mathbf{Z}_{uv} \cdot \mathbf{GR} \quad (29)$$

so,

$$T(p) = \xi(i_m, j_m, i_n, j_n)$$

where  $p$  yields (24).

(29) will largely reduce matrix filling time.

## 5. NUMERICAL EXAMPLES

To demonstrate applicability of the above formulation and to validate algorithms, numerical results for some scatters are presented and compare with available data in this section. All the examples are calculated on a PC with Pentium4 2.8 GHz CPU. The scatters are all illuminated by an incident plane wave. The calculated responses are back-scattered field.

As a first example, a perfectly conducting sphere is considered to validate the polynomial approximation method. The sphere has a radius of 0.06 m. The incident wave is  $x$ -polarized and  $z$ -traveling. The surface of sphere is divided into 584 triangles. Numerical tests, which are not particularly presented here, demonstrate that it is enough using about ten polynomials in (16). In this case,  $P = 8$ . The range of frequency is from 0.8 MHz to 3.9 GHz. 100 frequencies are extracted at equal intervals. Figure 1 compares the calculated monostatic RCS through Chebyshev polynomial approximation in MoM with that through Mie's series. The consuming time is 2 hours and 9 minutes. It takes about 15 hours and 10 minutes to compute point-by-point using the basic MoM. Clearly, the results presented in Figure 1 validate the fact, the numerical procedures employed in this work are accurate and take a much shorter period of time, and there are more triangles needed in high frequencies for more accurate results.

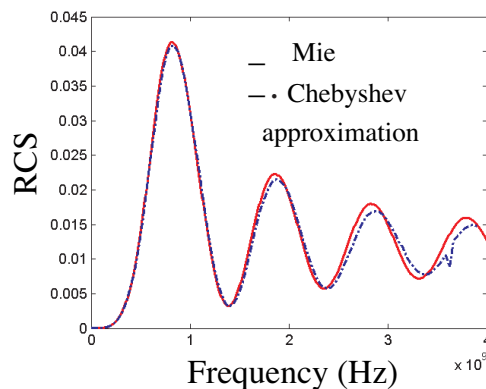


**Figure 1.** Monostatic RCS versus frequency for a conducting sphere.

The second example is a conducting square disk of  $1.0\lambda \times 1.0\lambda$ . The disk is four quadrilaterals meshed as shown in Figure 2. At different current order ( $M$ ) and corresponding number of integral nodes, the reference matrix filling time of direct numerical integration ( $T_D$ ) and by our method ( $T_{mat}$ ) are shown in Table 1. Clearly, the method in

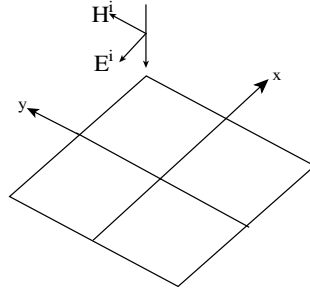


**Figure 2.** A meshed disk of  $1.0\lambda \times 1.0\lambda$ .

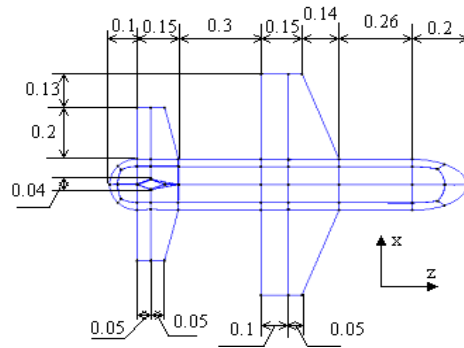


**Figure 3a.** The planform of the missile model.

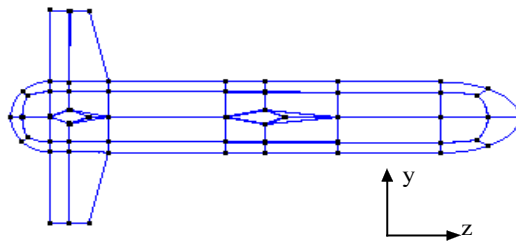


**Figure 3b.** The side view of the missile model.

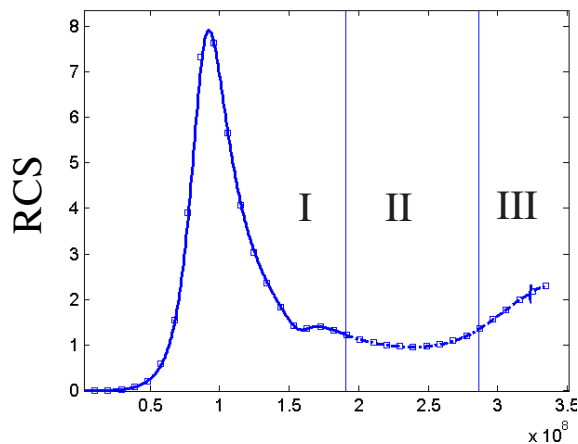
part 4 of this paper is much better.

The following example is a kind of missile model as shown in Figure 3a and Figure 3b. The unit of label is meter ( $m$ ). The main part is a circle cylinder. The front part is half a spheroids, and the tail is half a sphere.

The incident wave is  $z$ -polarized and  $x$ -traveling. Three different

**Table 1.** The matrix-filled time for the disk.

$M$	$N_{unk}$	$N_G$	$T_D$ (s)	$T_{mat}$ (s)
1	2	2	1	$\approx 0$
2	24	3	8	1
3	60	4	77	2
4	112	5	443	4

**Figure 4.** Monostatic RCS versus frequency for the missile model.

frequency bands are respectively considered in this example. As shown in Figure 4, the three bands are separated into I, II and III by beelines. Firstly, from 477 KHz to 191 MHz, 400 frequency points are sampled, and the interval is 477 KHz. The model is triangularized using 1132 patches. The method in part 3 is used. In (16),  $P = 8$ . And the result is line-plotted in part I of Figure 4. The taking time is 6 h 31 min. Secondly, from 191 MHz to 286 MHz, the same interval is chosen, and 200 frequency points are sampled. The model is meshed using 568 quadrilaterals. The rooftop basis functions and point-by-point method are used. And the result is shown as dash-dot line in part II of Figure 4. It takes 12 h 59 min. Lastly, from 286 MHz to 334 MHz, 100 frequency points are chosen by the same intervals. The model is meshed using 408 quadrilaterals. HO-MoM is used and the order of current is 2 ( $M = 2$ ). The time taken for calculation, part III of Figure 4, is 10 h 45 min. The comparing data are plotted as '□', obtained at 35 frequency points of equal interval from 477 KHz to 334 MHz, using rooftop basis functions

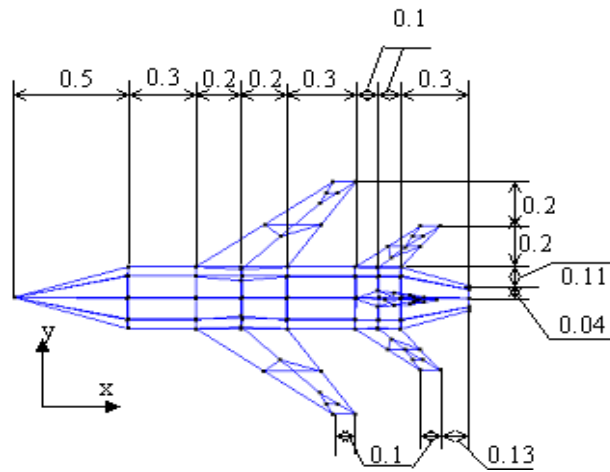


**Figure 5a.** The planform of the plane model.

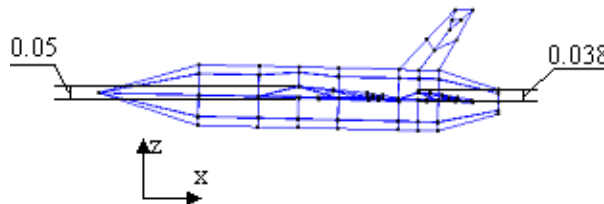


**Figure 5b.** The side view of the plane model.

of MoM with 918 quadrilaterals meshing.

Finally, a kind of aircraft model is as shown in Figure 5a and Figure 5b. The unit of label is meter. The main part is a circle cylinder. The front part is a circle cone, and the tail is a round dais.

The incident wave is  $x$ -polarized and  $z$ -traveling. Two different frequency bands are respectively considered in this case. As shown in Figure 6, the two bands are separated into I and II by a beeline. Firstly, from 477 KHz to 191 MHz, 400 frequency points are sampled, and the interval is 477 KHz. The model is triangularized using 1050 patches. The method in part 3 is used. And the response is line-plotted in part I of Figure 6. The taking time is 6 h 27 min. Secondly, from 191 MHz to 286 MHz, the same interval is chosen, and 200 frequency points are sampled. The model is meshed using 450 quadrilaterals. HO-MoM is used and the order of current is 2 ( $M = 2$ ). The time taken for calculation, dashed line in part II of Figure 6, is 35 h 49 min. The comparing data are plotted as '□', obtained at 30 frequency points of

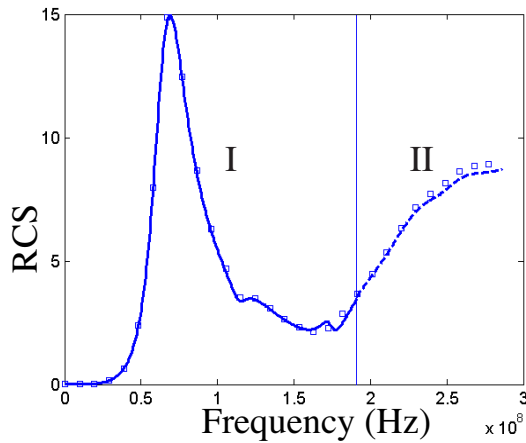


**Figure 6.** Monostatic RCS versus frequency for the plane model.

equal interval from 477 KHz to 286 MHz, using rooftop basis functions of MoM with 1242 quadrilaterals meshing.

## 6. CONCLUSIONS

In this work, a simple and efficient numerical technique is proposed to solve wide-band frequency responses of complex radar targets on a personal computer. In low frequency, the matrices from MoM can be rapidly filled at different frequencies by the Chebyshev polynomial approximation. When frequencies are relatively high, the HO-MoM is used at each frequency point. A fast method is proposed that matrices products are substituted for multi-dimension numerical integrations. For scatters in low and resonance frequency domain, which are in our interest, the numerical results by that procedure are accurate.

## REFERENCES

1. Darve, E., "The fast multipole method: numerical implementation," *Journal of Computational Physics*, Vol. 160, 195–240, 2000.
2. Song, J. M., C. C. Lu, W. C. Chew, and S. W. Lee, "Introduction to fast illinois solver code (FISC)," *IEEE Antennas Propagation Symposium*, 48–51, 1997.
3. Sertel, K. and J. L. Volakis, "Method of moments solution of volume integral equations using parametric geometry," *Radio Sci.*, Vol. 37, No. 1, 1–7, 2002.

4. Jørgensen, E., J. L. Volakis, P. Meincke, and O. Breinbjerg, "Higher order hierarchical Legendre basis functions for electromagnetic modeling," *IEEE Trans. Antennas Propagat.*, Vol. AP-52, No. 11, 2985–2995, Nov. 2004.
5. Djordjevic, M. and B. M. Notaroš, "Double higher order method of moments for surface integral equation modeling of metallic and dielectric antennas and scatters," *IEEE Trans. Antennas Propagat.*, Vol. 52, No. 8, 2118–2129, 2004.
6. Cockrell, C. R. and F. B. Beck, "Asymptotic waveForm evaluation (AWE) technique for frequency domain electromagnetic analysis," NASA Technical Memorandum 110292, 1996.
7. Reddy, C. J., "Application of model based parameter estimation for RCS frequency response calculations using method of moments," NASA/CR-1998-206951, 1998.
8. Rao, S. M., D. R. Wilton, and A. W. Glisson, "Electromagnetic scattering by surfaces of arbitrary shape," *IEEE Trans. Antennas Propagat.*, Vol. AP-30, No. 3, 409–418, May 1982.
9. Notaroš, B. M. and B. D. Popovic, "Optimized entire-domain moment-method analysis of 3D dielectric scatterers," *Int. J. Numerical Modelling: Electronic Networks, Devices and Fields*, Vol. 10, Nos. 5–6, 177–192, 1997.
10. Peterson, A. F., S. C. Ray, and R. Mittra, *Computational Methods for Electromagnetics*, IEEE Press, New York, 1998.